Large-scale 3D integral equation based inversion of EarthScope MT data using a variable sensitivity domain

Martin Čuma, Michael S. Zhdanov and Alexander V. Gribenko, University of Utah and TechnoImaging*

Summary

Moving sensitivity domain that varies with frequency was implemented and tested in a parallel magnetotelluric (MT) integral equation inversion. This approach reduces computation time and memory requirements. We assess the robustness of the approach by model tests and apply it to the inversion of EarthScope MT data collected over the Northwestern US. Prominent features obtained by this inversion include resistive structure associated with the Juan de Fuca slab subducting beneath the northwestern United States and the conductive zone of partially melted material above the subducting slab corresponding to the Cascade volcanic arc. We also observe extensive areas of moderate-to-high conductive asthenosphere below 100 to 200 km and high-conductive body associated with the Yellowstone mantle plume.

Method

In MT methods, the earth's natural electromagnetic field is used as a source field. The mutually orthogonal horizontal components of electric and magnetic fields are recorded on the earth's surface. The interpretation of magnetotelluric data is based on the calculation of the transfer functions between the horizontal components of the electric and magnetic fields, which form the magnetotelluric impedance tensor Z:

$$Z = \begin{bmatrix} Z_{xx} & Z_{xy} \\ Z_{yx} & Z_{yy} \end{bmatrix}. \quad (1)$$

In our MT inversion algorithm, we use the integral equation (IE) method for forward modeling. In the framework of this method, the EM field is presented as a sum of the background (normal) $\{\mathbf{E}^b, \mathbf{H}^b\}$ and anomalous $\{\mathbf{E}^a, \mathbf{H}^a\}$ fields:

$$\mathbf{E}= \mathbf{E}^b + \mathbf{E}^a, \mathbf{H}= \mathbf{H}^b + \mathbf{H}^a, \quad (2)$$

where the background field is a field generated by the given sources in the model with a background distribution of conductivity σ_b, and the anomalous field is produced by the anomalous conductivity distribution $\Delta\sigma_a$.

The process of solving the forward electromagnetic problem according to the integral equations consists of two parts. First, it is necessary to find the electric and magnetic fields inside the domain V (where $\Delta\sigma\neq0$), which requires the solution of an integral equation (*domain equation*) for $r'\in V$. Second, using the *data equations* with $r'\in P$, we calculate the EM field in the receiver domain P. Usually, the first part is more complicated and requires most of the computational time, because it consists of solving a large system of linear equations.

We can describe the forward MT problem by an operator equation:

$$\mathbf{d} = \mathbf{A}(\mathbf{m}), \quad (3)$$

where **d** stands for a data vector formed by the components of the MT impedances, and **A** is the nonlinear forward operator symbolizing the governing equations of the MT modeling problem. Equation 3 is ill posed, i.e., the solution can be nonunique and unstable. We use Tikhonov regularization, which is based on minimization of the parametric functional (Tikhonov and Arsenin, 1977, Zhdanov, 2002).

We solve this minimization problem by using the re-weighted regularized conjugate-gradient (RRCG) method with adaptive regularization parameter selection (Zhdanov, 2002). Calculation of the conjugate gradient requires obtaining the Fréchet derivative matrix of sensitivities for which we use quasi-Born approximation (Zhdanov, 2009), which reduces the amount of computations dramatically while retaining numerically stable solution.

The Fréchet derivative is the most expensive item in the inversion not only in terms of the computation time, but also in the computer memory required for its storage. The number of entries in the Fréchet derivative matrix is equal to the number of MT data points times the number of cells in the inversion domain. To reduce the storage and computation requirements, we use a moving sensitivity domain approach in our MT inversion (Zhdanov et al., 2010, 2012; Cox et al., 2010).

In the framework of the moving sensitivity approach, for a given receiver we compute and store the Fréchet derivative inside the inversion cells within a predetermined horizontal distance from this receiver only; i.e., within a sensitivity domain. Thus, Fréchet derivatives for an MT station can be computed and stored for regions much smaller than the entire inversion domain only. The sensitivity domain size is determined based on the rate of sensitivity attenuation of MT data. As the sensitivity attenuates faster for higher frequencies, we vary the domain size with frequency, which provides the optimal memory use and computation speed while retaining required accuracy. We apply the

DOI http://dx.doi.org/10.1190/segam2013-0300.1

moving sensitivity approach for the Fréchet derivative calculation and not for the computations of the predicted field. By using all of the cells in the forward modeling computations, we ensure an accurate result for the calculations of the predicted fields in the receivers.

Measured MT data accuracy tends to vary with the frequency. Low frequency data generally have larger errors due to longer time periods needed to collect statistically significant measurements. It is thus advisable to include some kind of accuracy information into the inversion process in order to weigh out the less accurate data. We utilize approach similar to Avdeev and Avdeeva (2009), where we include the covariance of the measured data into the data weights as:

$$W_d = \frac{1}{\beta_{jn}\|Z\|\sqrt{f}}, \quad (4)$$

where f is the frequency and the impedance norm is summed over all impedance components and stations for the given frequency. β_{jn} is the relative error of the observed impedance Z_{jn} defined as:

$$\beta_{jn} = \sqrt{\frac{\varepsilon_{jn}}{Z_{jn}^T Z_{jn}}}, \quad (5)$$

ε_{jn} is the reported impedance variance, and j and n are the impedance matrix component indices. These data weights are then utilized in the calculation of the data misfit as:

$$\varphi(\mathbf{m}) = |\mathbf{W}_{d,jn}\,[\mathbf{A}(\mathbf{m})-\mathbf{d}]|. \quad (6)$$

Our large-scale 3D MT data inversion is implemented as massively parallel software with two levels of MPI parallelization, the higher level parallelizes over the frequencies of the MT field, the lower level over the horizontal layers of the discretization grid. Furthermore, each MPI process can launch a number of OpenMP threads which in parallel compute the workload required for each process. On cluster computers, we typically map one MPI process per CPU socket and associate threads with CPU cores. This allows us to run the inversion efficiently on hundreds of cluster nodes and thousands of CPU

Inversion validation

We have assessed the reliability of our inversion approach by using numerous models, the most important of which we detail in this section. Response for all the models has been calculated using integral equations based PIE3D code (Čuma et. al, 2012).

Model 1 is a checkerboard test with 3x3x3 rhomboidal 1000 or 10 Ohm-m anomalies embedded in a 100 Ohm-m background. The domain is 1000x1000x500 km^3 and the anomalies are 300x300 km^2 horizontally and 20, 40 and 150 km vertically. MT receivers are spaced on a 70 km grid, similar to the EarthScope spacing, and we use 24 frequencies with periods from 19.7 to 7300 s, the same as in the EarthScope data. 3% Gaussian noise was added to the electromagnetic fields before calculating the impedances. Figure 1 shows the horizontal and vertical cross sections of the model. Figure 2 presents the full impedance inversion result. We can see that the inversion recovers the first anomaly layer quite well. In the second layer, the conductors show up very well while the resistors do not. The deepest anomaly layer shows a hint of the conductor between 200 and 350 km depth, which is expected due to shielding from the higher conductors.

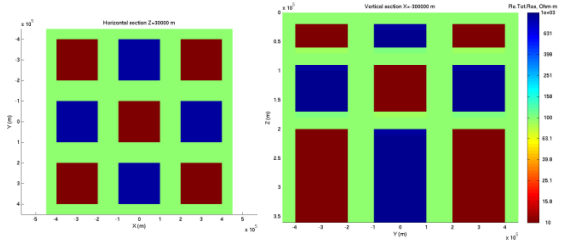

Figure 1: Horizontal (left) and vertical (right) cross sections of Model 1.

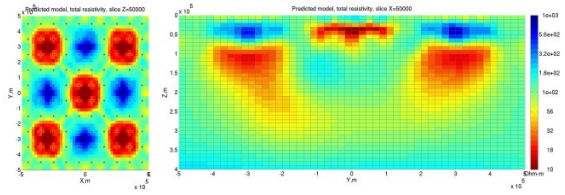

Figure 2: Horizontal cross section of the results of full impedance inversion for Model 1 at 50 km depth (left) and vertical cross section of the same model (right).

In order to evaluate the optimal size of the receiver sensitivity domain, which can vary with the frequency, we use Model 1 data and vary the maximum receiver sensitivity domain as a multiple of the skin depth at that frequency for the background resistivity of 100 Ohm-m. Figure 3 shows the horizontal cross section of the full impedance inverted model at 50 km depth. We set the sensitivity domain radius equal to the skin depth times a multiplier from 1 to 5. Notice that, the 1x skin depth sensitivity domain result is very grainy and unusable. The result with 2x skin depth sensitivity domain radius is better but there are still artifacts. The results with 3x and larger skin depth sensitivity domain radius are very close to the result with no sensitivity domain. We therefore conclude

DOI http://dx.doi.org/10.1190/segam2013-0300.1

that the optimal sensitivity domain radius is 3x the size of the skin depth.

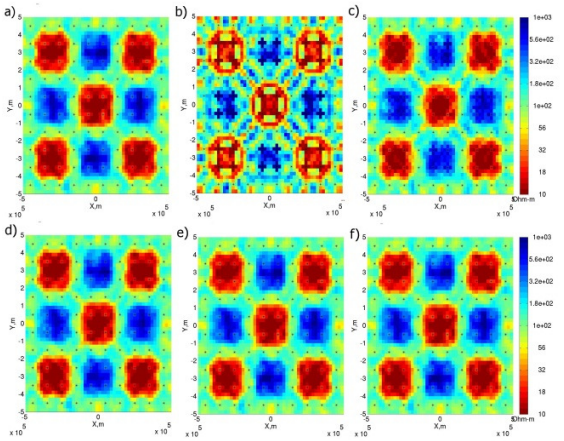

Figure 3: Horizontal cross section of inverted Model 1 at 50 km depth. a) no sensitivity domain (SD) b) SD radius of the size of skin depth c) 2x the skin depth d) 3x the skin depth e) 4x the skin depth f) 5x the skin depth.

Inversion of EarthScope MT data

EarthScope MT data collected over the northwestern United States include 330 stations. We filtered out some noisy stations and ended up 314-318 stations for each frequency. We use 24 frequencies ranging from 19.7 to 7300 s. The inversion domain was spanned in the X (geographic E-W), Y (geographic N-S), and Z (vertical downward) directions extending 1650 km, 1350 km, and 500 km, respectively. The domain cells had horizontal discretization of 10x10 km, and vertical discretization of 96 layers starting from 500 m at the surface and logarithmically increasing with depth. The inversion domain contained 2,138,400 cells, and had an initial model of a 100 ohm-m half space. We also include the ocean as an a priori model in the inversion domain, and also as an inhomogeneous background domain (Zhdanov et. al, 2006) for the area up to 500 km away from the inversion domain.

For the full impedance inversion result we present, we used 192 sixteen-core nodes, splitting the work into 384 MPI processes, each of which ran eight OpenMP threads, to a total of 3072 cores. It took about 10 hours to finish 48 iterations to obtain RMS of 2.56. Similarly to Meqbel et. al. (2012), the RMS was calculated assuming data error equal to 5% of the norm of the principle impedance values.

The conductivity distribution as recovered by our 3D inversion of data reflects the regional features. Figures 4 and 5 show horizontal cross sections of our geoelectric model at depths of 35 km, 80 km, 150 km and 300 km. The subducting Juan de Fuca slab (JDF) is clearly imaged in these horizontal sections. It is characterized by the zone of very high resistivity (~ 1000 ohm-m) shown by the dark blue color, which corresponds well to the known fact that the subducting oceanic lithosphere is very resistive (e.g., Wannamaker et al., 1989). There is also a hint of the division between the JDF Plate, Gorda Plate and Pacific Plate revealed by higher conductivity in area of south-western Oregon.

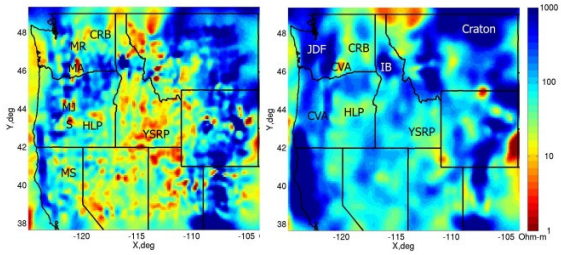

Figure 4: Horizontal cross sections of the EarthScope model at 35 km depth (left) and 80 km depth (right).

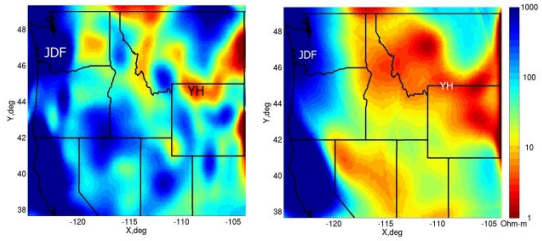

Figure 5: Horizontal cross sections of the EarthScope model at 150 km depth (left) and 300 km depth (right).

There are several crustal conductors: HLP extends under the High Lava Plains and CRB extends beneath the Columbia River basalts. These anomalies are associated with the heating processes from the subducting oceanic slabs (Roth et. al., 2008). Another conductive lineament extends beneath Yellowstone - Snake River Plain (YSRP). This conductive structure is associated with the tomographically imaged mantle plume-like layer emerging from the upper mantle toward the Yellowstone volcano (e.g., Schutt et al., 2008; Smith et. al., 2009, Schmandt and Humphreys, 2010; Zhdanov et al., 2011). Similar to the slow velocity anomaly imaged by James et al. (2011), the conductive plume is in fact a mantle layer that extends in a southwest direction into eastern Idaho.

We also observe a resistive anomaly beneath the northern Idaho close to the Idaho Batholith (IB) near the margin of Precambrian North America. Notably, this resistive zone corresponds to the region of increased (~2%) velocities

DOI http://dx.doi.org/10.1190/segam2013-0300.1

described by Roth et al. (2008). Another explanation for this resistor has been recently suggested by Schmandt and Humphreys (2011), arguing that this resistor is due to fragmented oceanic lithosphere slab that has been twisted and lifted up by subsequent Juan de Fuca plate subduction from the west. To the northeast we notice prominent resistors consistent with the Wyoming Craton (WC) and the Medicine Hat Craton (MHC).

Turning to the shallower features at 35 km depth in Figure 4, notice several strong conductors in the west corresponding to the Cascadia Volcanic Arc (CVA) volcanoes (Mt. Rainer - MR, Mt. St. Helens - Mt. Adams - MA, Mt. Jefferson - MJ, Sisters -S, Mt. Shasta - MS, Lassen Pk. - LP), with the most prominent large conductor under the Mt. St. Helens - Mt. Adams complex (MA). There are also localized conductors in the Great Basin, and northern Rockies area and a prominent conductive area corresponding to the Yellowstone - Snake River Plain. Resistive features are again apparent in the northeastern cratons and under the western Colorado and central Wyoming.

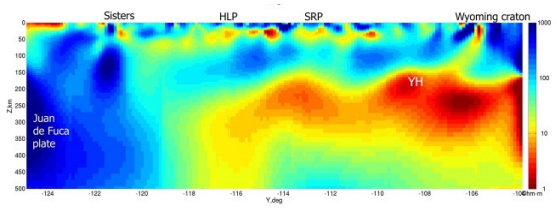

Figure 6: Vertical cross section of the EarthScope model at 44N

Figure 6 shows vertical slice along 44 N. The subducting oceanic plate is clearly imaged in the west. We can also see the conductive zone of partially melted material directly above the subducting slab, which can be explained by the release of fluids from the down-going slab. The conductor in this cross section is in the vicinity of the Sisters volcano. There are also large zones of moderate-to-high conductivity (~5-10 ohm-m) below 100-200 km in the upper mantle, which represent the electrical properties of the conductive electrical asthenosphere (CA).

Another remarkable geoelectrical feature shown in the vertical resistivity sections is an extensive area of low resistivity (~ 1-10 ohm-m) in the upper mantle, and in some parts, in the low crust, which extends beneath the northwest Basin and Range (BR), High Lava Plains (HLP), Snake River Plain (SRP), and Blue Mountains (BM). Note that, a similar result was observed by Patro and Egbert (2008) and Meqbel et. al. (2012) using finite difference based 3D inversion of the EarthScope MT data. Interestingly, as early as in 1977, Stanley et al. (1977) conducted MT soundings along a profile extending from the Raft River geothermal area in southern Idaho to Yellowstone National Park in Wyoming. The 1D interpretation of these MT sounding curves revealed a highly conductive crustal anomaly with the depth of the conductive zone about 25 km depth and the resistivity less than 10 0hm-m and at some sites less than 1 0hm-m.

Conclusions

We have inverted the EarthScope MT data acquired to the end of 2011 over the northwestern United States. Similar to published seismic tomography models (Obrebski et. al, 2010, 2011), our inverse geoelectrical model of the Earth's interior beneath the northwestern United States shows a resistive structure associated with the Juan de Fuca slab subducting beneath the Precambrian northwestern United States, and the conductive anomalies characterizing the partially melted material above the subducting slab. The geoelectrical model also contains several prominent conductive features, such as conductive lineaments beneath the High Lava Plains and the Snake River Plain, the conductivity anomaly extending beneath the Columbia River basalts, the conductive mantle layer of the Yellowstone hotspot, and extensive areas of low resistivity in the upper mantle and in the low crust.

In conclusion, we acknowledge that our geoelectrical model of the northwestern United States represents just one of the first models obtained from 3D inversion of EarthScope MT data. Such large-scale MT inversions are extremely complex, and require significant efforts to fully model, understand, and interpret. The focus of future research should be on the integrated interpretation of seismic, electromagnetic, gravity, magnetic, and geothermal data, which would reduce ambiguity of geophysical inversion.

Acknowledgements

The authors acknowledge the support of the University of Utah Consortium for Electromagnetic Modeling and Inversion (CEMI). The MT data were acquired by the Incorporated Research Institutions for Seismology (IRIS) as part of the operation of the USArray. Data used in this study were made available through EarthScope (www.earthscope.org; EAR-0323309), supported by the National Science Foundation. We also acknowledge allocation of computer time provided by the University of Utah's Center for High Performance Computing (CHPC) and the Texas Advanced Computing Center (TACC). We also acknowledge TechnoImaging for support of this research. We further thank Marie Green, Muran Han and Yue Zhu for assistance with some of the model studies and figures.

DOI http://dx.doi.org/10.1190/segam2013-0300.1

http://dx.doi.org/10.1190/segam2013-0300.1

EDITED REFERENCES

Note: This reference list is a copy-edited version of the reference list submitted by the author. Reference lists for the 2013 SEG Technical Program Expanded Abstracts have been copy edited so that references provided with the online metadata for each paper will achieve a high degree of linking to cited sources that appear on the Web.

REFERENCES

Avdeev, D., and A. Avdeeva, 2009, 3D magnetotelluric inversion using a limited-memory quasi-Newton optimization: Geophysics, **74**, no. 3, F45–F57, http://dx.doi.org/10.1190/1.3114023.

Cox, L. H., G. A. Wilson, and M. S. Zhdanov, 2010, 3D inversion of airborne electromagnetic data using a moving footprint: Exploration Geophysics, **41**, no. 4, 250–259, http://dx.doi.org/10.1071/EG10003.

Cuma, M., M. S. Zhdanov, and K. Yoshioka, 2013, Parallel integral equation 3D (PIE3D) 2012: Presented at the Annual Meeting, Consortium for Electromagnetic Modeling and Inversion (CEMI).

Endo, M., M. Cuma, and M. S. Zhdanov, 2009, Large-scale electromagnetic modeling for multiple inhomogeneous domains: Communications in Computational Physics, **6**, 269–289, http://dx.doi.org/10.4208/cicp.2009.v6.p269.

James, D. E., M. J. Fouch, R. W. Carlson, and J. B. Roth, 2011, Slab fragmentation, edge low and the origin of the Yellowstone hotspot track: Earth and Planetary Science Letters, **311**, no. 1-2, 124–135, http://dx.doi.org/10.1016/j.epsl.2011.09.007.

Meqbel, N., G. D. Egbert, P. Wannamaker, and A. Schultz, 2012, Three dimensional conductivity models of the northwestern US derived from 3-D inversion of USArray magnetotelluric data: Presented at the 21st EM Induction Workshop, S5-3.

Obrebski, M., R. M. Allen, F. Pollitz, and S. H. Hung, 2011, Lithosphere–asthenosphere interaction beneath the western United States from the joint inversion of body-wave traveltimes and surface-wave phase velocities: Geophysical Journal International, **185**, 1003–1021, http://dx.doi.org/10.1111/j.1365-246X.2011.04990.x.

Obrebski, M., R. M. Allen, M. Xue, and S. H. Hung, 2010, Slab-plume interaction beneath the Pacific Northwest: Geophysical Research Letters, **37**, no. 14, L14305, http://dx.doi.org/10.1029/2010GL043489.

Patro, P. K., and G. D. Egbert, 2008, Regional conductivity structure of Cascadia: Preliminary results from 3D inversion of USArray transportable array magnetotelluric data: Geophysical Research Letters, **35**, no. 20, L20311, http://dx.doi.org/10.1029/2008GL035326.

Roth, J. B., M. J. Fouch, D. E. James, and W. Carlson, 2008, Three-dimensional seismic velocity structure of the northwestern United States: Geophysical Research Letters, **35**, no. 15, L15304, http://dx.doi.org/10.1029/2008GL034669.

Schmandt, B., and E. Humphreys, 2010, Complex subduction and small-scale convection revealed by body-wave tomography of the western United States upper mantle: Earth and Planetary Science Letters, **297**, no. 3-4, 435–445, http://dx.doi.org/10.1016/j.epsl.2010.06.047.

Schmandt, B., and E. Humphreys, 2011, Seismically imaged relict slab from the 55 Ma Siletzia accretion to the northwest United States: Geology, **39**, no. 2, 175–178, http://dx.doi.org/10.1130/G31558.1.

Schutt, D. L., K. Dueker, and H. Yuan, 2008, Crust and upper mantle velocity structure of the Yellowstone hot spot and surroundings: Journal of Geophysical Research, **113**, no. B3, B03310, http://dx.doi.org/10.1029/2007JB005109.

Smith, R. B., M. Jordan, B. Steinberger, C. M. Puskas, J. Farrell, G. P. Wait, S. Husen, W. L. Chang, and R. O'Connell, 2009, Geodynamics of the Yellowstone hotspot and mantle plume: Seismic and GPS imaging, kinematics, and mantle flow: Journal of Volcanology and Geothermal Research, **188**, no. 1-3, 26–56, http://dx.doi.org/10.1016/j.jvolgeores.2009.08.020.

Tikhonov, A. N., and V. Y. Arsenin, 1977, Solution of ill-posed problems: V. H. Winston and Sons.

Wannamaker, P. E., J. R. Booker, A. G. Jones, A. D. Chave, J. H. Filloux, H. S. Waff, and L. K. Law, 1989, Resistivity cross section through the Juan de Fuca subduction system and its tectonic implications: Journal of Geophysical Research, **94**, no. B10, 14127–14144, http://dx.doi.org/10.1029/JB094iB10p14127.

Yuan, H., and K. Dueker, 2005, Teleseismic *P*-wave tomogram of the Yellowstone plume: Geophysical Research Letters, **32**, no. 7, L07304, http://dx.doi.org/10.1029/2004GL022056.

Zhdanov, M. S., 2002, Geophysical inverse theory and regularization problems: Elsevier.

Zhdanov, M. S., 2009, Geophysical electromagnetic theory and methods: Elsevier.

Zhdanov, M. S., A. Green, A. Gribenko, and M. Cuma, 2010, Large-scale three-dimensional inversion of Earthscope MT data using the integral equation method: Physics of the Solid Earth, **46**, no. 8, 670–678.

Zhdanov, M. S., A. Gribenko, M. Cuma, and M. A. Green, 2012, Geoelectrical structure of the lithosphere and asthenosphere beneath the northwestern United States: Journal of Geology and Geosciences, **1**, 1–6, http://dx.doi.org/10.4172/jgg.1000106.

Zhdanov, M. S., S. K. Lee, and K. Yoshioka, 2006, Integral equation method for 3D modeling of electromagnetic fields in complex structures with inhomogeneous background conductivity: Geophysics, **71**, no. 6, G333–G345, http://dx.doi.org/10.1190/1.2358403.

Zhdanov, M. S., R. B. Smith, A. Gribenko, M. Cuma, and M. Green, 2011, Three-dimensional inversion of large-scale EarthScope magnetotelluric data based on the integral equation method: Geoelectrical imaging of the Yellowstone conductive mantle plume: Geophysical Research Letters, **38**, no. 8, L08307, http://dx.doi.org/10.1029/2011GL046953.